Monthly Notices of the ROYAL ASTRONOMICAL SOCIETY
MNRAS **457,** 1916–1930 (2016) doi:10.1093/mnras/stw130

The fate of high-redshift massive compact galaxies

Ignacio G. de la Rosa,[1,2]★ Francesco La Barbera,[3] Ignacio Ferreras,[4] Jorge Sánchez Almeida,[1,2] Claudio Dalla Vecchia,[1,2] Inma Martínez-Valpuesta[1,2] and Martin Stringer[1,2]

[1]*Instituto de Astrofísica de Canarias, C/ Vía Láctea s/n, E-38205 La Laguna, Tenerife, Spain*
[2]*Departamento de Astrofísica, Universidad de La Laguna, E-38206 La Laguna, Tenerife, Spain*
[3]*INAF – Osservatorio Astronomico di Capodimonte, Napoli, I-80131, Italy*
[4]*Mullard Space Science Laboratory, University College London, Holmbury St Mary, Dorking, Surrey RH5 6NT, UK*

Accepted 2016 January 13. Received 2015 December 24; in original form 2015 July 30

ABSTRACT

Massive high-redshift quiescent compact galaxies (nicknamed *red nuggets*) have been traditionally connected to present-day elliptical galaxies, often overlooking the relationships that they may have with other galaxy types. We use large bulge–disc decomposition catalogues based on the Sloan Digital Sky Survey to check the hypothesis that red nuggets have *survived* as compact cores embedded inside the haloes or discs of present-day massive galaxies. In this study, we designate a *compact core* as the bulge component that satisfies a prescribed compactness criterion. Photometric and dynamic mass–size and mass–density relations are used to show that, in the inner regions of galaxies at $z \sim 0.1$, there are *abundant* compact cores matching the peculiar properties of the red nuggets, an abundance comparable to that of red nuggets at $z \sim 1.5$. Furthermore, the morphology distribution of the present-day galaxies hosting compact cores is used to demonstrate that, in addition to the standard channel connecting red nuggets with elliptical galaxies, a comparable fraction of red nuggets might have ended up embedded in discs. This result generalizes the inside-out formation scenario; present-day massive galaxies can begin as dense spheroidal cores (red nuggets), around which *either* a spheroidal halo or a disc is formed later.

Key words: galaxies: bulges – galaxies: evolution – galaxies: formation – galaxies: stellar content – galaxies: structure.

1 INTRODUCTION

An approximate census of massive galaxies at redshift $z \sim 1.5$ provides a morphological classification into 40 per cent discs, 15 per cent extended spheroids, 25 per cent compact spheroids and 20 per cent peculiar objects (e.g. Peth et al. 2015). More than 9 Gyr later, in the present-day Universe, a similar census of massive galaxies gives 30 per cent discs, 65 per cent extended spheroids and 5 per cent peculiar morphologies. Strikingly, compact spheroids are virtually absent in the present-day Universe (e.g. Trujillo et al. 2009; Taylor et al. 2010; Saulder, van den Bosch & Mieske 2015). At $z \sim 1.5$, the majority (∼80 per cent) of massive compact spheroids were already quiescent, while the rest were actively forming stars. The massive high-redshift quiescent compact galaxies have been termed *red nuggets* (Damjanov et al. 2009). Recent studies on the number density evolution of red nuggets point to the star-forming compact massive galaxies (sCMGs) as their probable progenitors (e.g. Barro et al. 2013; van Dokkum et al. 2015, hereafter vDokkum15). At redshift $z \sim 2.5$, the number density of sCMGs matched that of red nuggets. By $z \sim 1.5$, 1.5 Gyr later, the number density of red nuggets has increased by an order of magnitude while that of sCMGs has decreased by a factor of 2. The straightforward interpretation is that the red nuggets are the descendants of rapidly quenched sCMGs. But unlike this relative consensus on the origin of red nuggets, there is not the same agreement regarding their fate after $z \sim 1.5$.

Red nuggets were discovered almost a decade ago (e.g. Daddi et al. 2005; Trujillo et al. 2006a; Longhetti et al. 2007), and more than a hundred studies have been carried out on their evolution. Since their discovery, red nuggets have been linked to present-day elliptical galaxies; the two classes share a similar spheroidal morphology, and the fraction of elliptical galaxies (extended spheroids) has increased by a factor of 4 in the last 9 Gyr (Buitrago et al. 2013). But for the former population to have evolved into the latter, there must be a mechanism by which an ultra-compact spheroid with half-light radius of ∼1 kpc can become a fully fledged elliptical, three to six times larger. Several physical processes, including major and minor mergers (e.g. Naab, Johansson & Ostriker 2009;

★ E-mail: irosa@iac.es

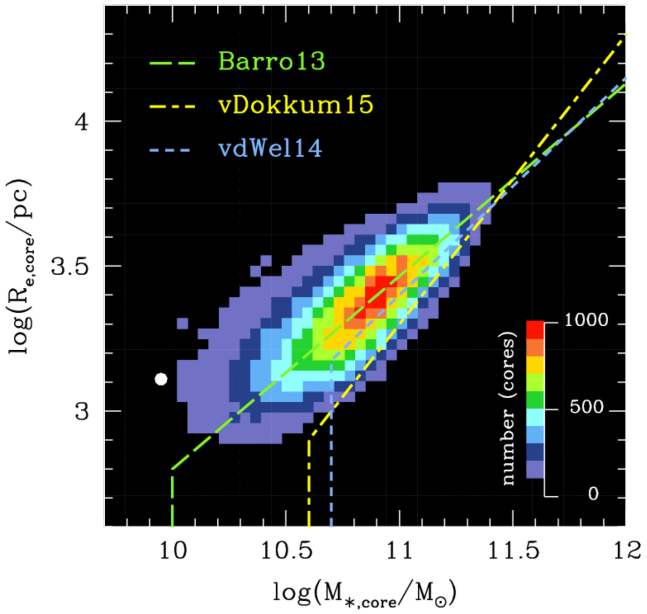

Figure 1. Bidimensional histogram showing the mass–size distribution for all the decomposed cores in our sample galaxies (203 369 objects, see Table 1). Three compactness criteria, Barro13, vDokkum15 and vdWel14 (described in the text), are overplotted and compact cores are located below the dashed lines, rendering 65 637 systems under the Barro13 criterion. The more restrictive vDokkum15 and vdWel14 criteria render 10 566 and 12 721, respectively. Note that the vdWel14 line is only approximate, because the criterion requires major-axis sizes instead of the circularized radii used in the plot. The isolated white dot marks the approximate location of the Milky Way's bulge (e.g. Di Matteo et al. 2015; Licquia & Newman 2015).

Trujillo, Ferreras & de la Rosa 2011) and puffing-up by active galactic nucleus (AGN) activity (Fan et al. 2008), have been proposed to explain the considerable growth in size. The prevailing paradigm, put forward by Hopkins et al. (2009) and Bezanson et al. (2009), postulates an appealing scenario in which red nuggets ended up in the centres of present-day giant ellipticals. This proposal is consistent with the inside-out growth scenario (e.g. Loeb & Peebles 2003) in which compact cores are formed at high redshift ($z \geq 2$) through highly dissipative processes (e.g. Naab et al. 2007; Dekel et al. 2009; Oser et al. 2010; Johansson, Naab & Ostriker 2012) and then grow an extended stellar halo through dissipation-less minor mergers (e.g. Ferreras et al. 2014; Morishita & Ichikawa 2016).

In addition to this traditional evolutionary scenario, there is another potentially important channel leading from red nuggets to disc galaxy bulges. The pieces of main observational evidence for this scenario have been provided by Graham (2013), Dullo & Graham (2013) and Graham, Dullo & Savorgnan (2015). Graham (2013) sample includes the set of 19 red nuggets observed by Damjanov et al. (2009) and a catalogue of few hundred bulges compiled by Graham & Worley (2008). In two subsequent studies, Dullo & Graham (2013) and Graham et al. (2015) carried out detailed bulge+disc (B+D) decompositions, but only for a small sample of present-day S0 galaxies, finding that S0 bulges are structurally similar to red nuggets. Based on cosmological simulations, Zolotov et al. (2015) and Tacchella et al. (2015) show that extended star-forming discs develop around red nuggets after compaction.

Fig. 1 of Graham (2013) presents an instructive sketch of mass–size and mass–density diagrams for all the spheroidal families, from giant elliptical galaxies to globular clusters. In the accompanying text, the author emphasizes the considerable overlap of the structural properties of red nuggets with those of present-day bulges.

The aim of the present study is to carry out a comprehensive analysis of the connection between red nuggets and present-day compact cores without any restriction on the morphology of the host galaxies. Specifically, the hypothesis we want to test is that a significant fraction of red nuggets have *survived*, masked inside spheroidal or disc galaxies in the present-day Universe.

To support this hypothesis, we would need to find a sufficient population of compact cores embedded inside present-day galaxies, where

(i) *Core* is a generalization of the bulge component in B+D decomposition of galaxies with all morphologies.

(ii) *Compact core* is a core that fulfils the same compactness criterion used for red nuggets. We test the robustness of our results using three different definitions of compactness, from the literature.

(iii) *Sufficient* means that the abundance of present-day red nugget-like cores should be approaching[1] that of the red nuggets at $z \sim 1.5$.

The present study takes advantage of Sloan Digital Sky Survey (SDSS)-based catalogues containing B+D decomposition of hundreds of thousands of galaxies (e.g. Simard11; Meert et al. 2015). In particular, we have used the Mendel et al. (2014) catalogue, itself a derivation of Simard11, which provides stellar masses for the B and D structural components. We impose the B+D decomposition on the entire present-day galaxy sample, regardless of their morphology, designating as *cores* both the central components of ellipticals and the bulges of disc galaxies. After B+D decomposition, cores are treated as independent structures and evaluated for their compactness, according to standard criteria (see Section 2).

The layout of the paper is the following: Section 2 is devoted to the data description, including the selection of the $z \sim 0$ compact core sample, reference elliptical galaxies and the compilation of red nuggets from the literature. Section 3 is devoted to the results of the present study, in particular the check of the working hypothesis, i.e. that red nuggets have survived as the compact cores of present-day galaxies. Discussion and conclusions follow in Sections 4 and 5. Decimal logarithms are used along the study. To keep consistency with other studies, we assume a Λ cold dark matter cosmology with $\Omega_\Lambda = 0.7$, $\Omega_M = 0.3$ and $H_0 = 70$ km s^{-1} Mpc^{-1}.

2 THE DATA

Several samples are extracted from the parent catalogue (Mendel et al. 2014). First, we introduce the compactness criteria, which allow the selection of structurally similar cores and red nuggets. Secondly, low-redshift samples, namely the compact cores and reference ellipticals, are introduced and thirdly, the high-redshift red nugget sample is presented.

2.1 Compactness criteria

Our goal is to measure the abundance of $z \sim 0.1$ galaxy cores structurally similar to red nuggets, and compare it to that of red nuggets at $z \sim 1.5$. Therefore, information on the red nugget number density as

[1] Based on cosmological simulations (Furlong et al. 2015; Wellons et al. 2016), we might expect ∼20 per cent of the red nuggets to have been consumed or destroyed in merger events, so the abundances should not necessarily match exactly.

a function of redshift becomes crucial for our work. Three different studies have addressed this issue in the literature, based on different criteria to define the red nuggets. As emphasized by Damjanov et al. (2015), the galaxy number densities and the structural parameters are rather sensitive to the choice of the compactness criterion, as well as to the stellar mass range probed. Consequently, we have to assure that each comparison is carried out under the same selection criteria.

In the present study, circularized half-light radii R_e have been used, with

$$\log(R_e) = \log(R_{e,a}) + 0.5\log(b/a), \quad (1)$$

where $R_{e,a}$ is the half-light radius along the major axis and (b/a) is the axial ratio of the galaxy.

In order to test the robustness of our results, we compute the number density of red nuggets using three alternative definitions of compactness.

(i) The criterion proposed by Barro et al. (2013, hereinafter Barro13), used by several authors (e.g. Poggianti et al. 2013; Barro et al. 2015; Damjanov et al. 2015),

$$\log(R_e/\mathrm{kpc}) < (\log(M_\star/\mathrm{M}_\odot) - 10.3)/1.5. \quad (2)$$

This is generally associated with a mass limit $\log(M_\star/\mathrm{M}_\odot) \geq 10.0$.

(ii) A more restrictive compactness criterion, proposed by van Dokkum et al. (2015, hereinafter vDokkum15),

$$\log(R_e/\mathrm{kpc}) < \log(M_\star/\mathrm{M}_\odot) - 10.7, \quad (3)$$

with a $\log(M_\star/\mathrm{M}_\odot) \geq 10.6$ limit.

(iii) Finally, the criterion proposed by van der Wel et al. (2014, hereinafter vdWel14)

$$R_{e,a}/(M_\star/10^{11}\mathrm{M}_\odot)^{0.75} < 2.5\,\mathrm{kpc}, \quad (4)$$

with a $\log(M_\star/\mathrm{M}_\odot) \geq 10.7$ limit. It is worth mentioning that this criterion uses $R_{e,a}$, the half-light radius measured along the galaxy major axis, instead of the more common circularized radius, R_e.

While we test our results on the abundances of red nuggets and compact cores using all three different sets of selection criteria (Section 3.3), for the first part of this paper (Sections 3.1–3.2) we adopt the vDokkum15 definition. In fact, the definition of vdWel14 would not allow us to perform a direct comparison to other spheroidal systems (Section 3.1) as it is based on major-axis effective radii. On the other hand, the lower mass cutoff of Barro13 would imply a significantly higher contamination from star-forming galaxies in our sample of red nuggets, with respect to the vDokkum15 higher mass cutoff (see Moresco et al. 2013).

2.2 Low-redshift samples

The parent sample used in our study is the Mendel et al. (2014) catalogue (hereafter Mendel14), an upgraded section of the Simard et al. (2011) catalogue (Simard11), which contains the B+D decomposition of more than one million SDSS-DR7 galaxies. The main improvement to the original catalogue is the stellar mass calculation of the bulge and disc components. Stellar masses are computed through Spectral Energy Distribution (SED) fitting to the five SDSS *ugriz* bands, using dusty synthetic templates from Conroy, Gunn & White (2009) with a Chabrier (2003) stellar initial mass function (IMF). The Mendel14 catalogue includes 657 996 galaxies from the SDSS-DR7 (Abazajian et al. 2009) with spectroscopic redshifts and successful *ugriz* B+D decomposition available. The original 2D decomposition in Simard11 used three alternative galaxy fitting models:

(i) de Vaucouleurs bulge (fixed Sérsic index $n_{bulge} = 4$) + exponential disc (Sérsic index $n_{disc} = 1$),

(ii) exponential disc + free-n_{bulge}, with n_{bulge} allowed to vary from 0.5 to 8 and

(iii) a single-component free-n Sérsic model to fit the whole galaxy (n Sérsic).

It is important to notice that Mendel14 stellar masses were computed using only two of those fitting models: (ii) and (iii). The bias introduced by the use of (i) instead of (ii) is discussed in Appendix B.

Two low-redshift subsamples are extracted from the Mendel14 catalogue. The main one is the *compact core* subsample (Section 2.2.1), including galaxy cores that fulfil the vDokkum15 compactness criterion. The second subsample consists of bona fide ellipticals (Section 2.2.2), and serves as a reference point for the study of galaxy structural properties (Section 3.1).

Bulge–disc decomposition is a delicate procedure demanding extra care to guarantee reliable outcomes. We have applied a rigorous screening, with eight steps, generally following the recommendations of the catalogue authors (e.g. Berg et al. 2014; Bluck et al. 2014; Mendel14).

2.2.1 *Compact core subsample selection*

We select compact cores from the Mendel14 catalogue based on different criteria. This is summarized in Table 1, where we also report the number of objects surviving each selection step.

First, we adopt a surface brightness limit of $\mu_{50,r} \leq 23.0$ mag arcsec^{-2} to assure a complete sample. Although the formal surface brightness limit of the SDSS spectroscopic sample is $\mu_{50,r} = 24.5$ mag arcsec^{-2} (Strauss et al. 2002), the sample in the range $\mu_{50,r}$ 23.0–24.5 mag arcsec^{-2} is not complete because galaxies were targeted only under some particular local sky conditions. Secondly, we exclude objects with uncertain decomposition, using the parameter dBD, which is the offset between two alternative galaxy mass calculations, $M_B + M_D$ (sum of independently derived bulge and disc masses) and M_{B+D} (mass derived from the total bulge+disc photometry) in units of the standard error. Significant inequality between these two masses is an indication of inconsistent decomposition, so systems with the cutoff dBD $> 1\sigma$, proposed by Mendel14, are excluded. These two cuts removed 9.5 per cent of the objects, as seen in Table 1.

Table 1. Subsample selection, listing the steps leading from the parent sample (Mendel14) to our *compact core* subsample. Steps are described in the main text.

Filters	Objects
Parent sample (Mendel14)	657 996
Surface brightness	655 530
Uncertain decomposition	595 402
$0.025 \leq z \leq 0.15$	456 169
Type $\neq 4$	437 089
Disc(i) $\leq 60^o$	291 192
$e_{core} < 0.6$	249 990
$(R_{core}/\mathrm{PSF}) \geq 0.8$	203 369
Compact cores (vDokkum15)	10 566
Compact cores (Barro13)	65 637
Compact cores (vdWel14)	12 721

The third cutoff, limiting the redshift range, is set to achieve a significant sample completeness in terms of the core stellar mass, $M_{\star,\,\mathrm{core}}$, the main reference parameter of this study. The choice of redshift range, $0.025 \leq z \leq 0.15$, yields a significant completeness in our target mass range, $\log(M_{\star,\,\mathrm{core}}/\mathrm{M}_{\odot}) \geq 10.0$, as discussed in Appendix A. Notice that in the number density estimations (Section 3.3), the V/V_{max} statistic is also used to correct for any residual incompleteness.

In the fourth step, we exclude galaxies reported to show anomalous B+D decomposition, tagged 'Type-4' in the Mendel14 classification. They comprise galaxy/star superposition and inverted B+D profiles, in which a disc dominates at the centre and a bulge at the external parts. Following Berg et al. (2014), fifth and sixth cutoffs were applied to promote face-on inclinations and to avoid strong bars. Face-on galaxies (disc inclination ≤ 60 deg) are favoured in order to minimize internal disc extinction on the bulge light, while high bulge ellipticities are avoided to prevent strong bars being mistaken for bulges ($\mathrm{e}_{\mathrm{core}} < 0.6$).

Finally, the potential impact of poorly resolved galaxy images on the B+D decomposition is considered. We follow the study by Gadotti (2008), which showed that the structural properties of cores can be reliably retrieved provided that their effective radii are larger than ∼80 per cent of the point spread function (PSF) half-width at half-maximum, i.e. $(R_{\mathrm{e,\,core}}/\mathrm{PSF}) \geq 0.8$. So far, by imposing these seven selection criteria, the parent sample has been reduced to 203 369 objects (31 per cent of the original sample; see Table 1). The last selection is on the cores that fulfil the vDokkum15 compactness criterion (equation 3). Additionally, Table 1 shows the corresponding results for the other criteria (equations 2 and 4). Fig. 1 provides a visual display of the compact core selection criteria for both Barro13 and vDokkum15 on top of a 2D histogram including the 203 369 objects, which got through the first seven screening steps.

The *compact core* definition is essential to the present study and deserves further clarification. The B+D decomposition is straightforward for disc galaxies, where a compact core is simply a bulge that has satisfied the compactness criterion. A decomposed elliptical galaxy should not be interpreted literally as having physically meaningful bulge and a disc. In addition to the central *core*, the external component can be a disc, a halo or any significant departure from a single fit. Distinct inner components have been extensively observed in ellipticals (e.g. Côté et al. 2006; Lauer et al. 2007). More recently, Huang et al. (2013) have shown that more than 75 per cent of their sample of 94 nearby elliptical galaxies were better described when additional subcomponents were added to the conventional single Sérsic function.

We notice that some of the selection steps in Table 1 might bias our compact core abundance estimates. For instance, while the use of a given redshift range is not expected to impact our results, selections based on core elongation and SDSS image resolution might exclude some genuine compact cores from the number density estimates. Therefore, one should regard abundance estimates based on the compact core sample in Table 1 as lower limits. In Section 3.3, we discuss how removing some selection steps listed in Table 1 can be used to obtain upper limits on the number densities.

2.2.2 *The reference elliptical galaxies*

Throughout this study, the cores resulting from galaxy decomposition are treated as if they were independent spheroids detached from their surrounding haloes or discs. We compare the properties of these compact cores with a reference sample of bona fide ellipticals.

Bona fide ellipticals are selected from the subsample of 456 169 galaxies obtained after applying the first three selections listed in Table 1 to the Mendel14 catalogue. *Reference elliptical galaxies* have been selected according to their morphology and the type of fitted surface brightness profiles. We require the galaxy morphology to be *elliptical* according to the definitions given in Section 3.3 and Table 4. Additionally, ellipticals must belong to the *Type 1*, one of the four classes devised by Mendel14 to divide galaxies according to their profile. *Type 1* are single-component galaxies, in which the bulge component dominates the surface brightness profile at all radii (i.e. B/T ∼ 1). The resulting sample contains 18 916 elliptical galaxies. Size and mass parameters for these reference ellipticals are taken from the whole galaxy fit, using single-component, free-n Sérsic models. Note that a small fraction of ellipticals (∼4.5 per cent) are found to host a compact core. However, this does not affect our conclusions, our main aim being to compare the properties of ellipticals as a whole with those of compact cores, seen as separate structures, and red nuggets.

2.3 The red nugget sample

Our sample includes observed red nuggets from 29 works in the literature, 24 of which were part of two major compilations by Damjanov et al. (2011) and van de Sande et al. (2013), who renormalized them to a common observational frame. Damjanov et al. (2011) contributed 433 galaxies with spectroscopic redshifts spanning a range $0.18 \lesssim z \lesssim 2.67$. Their compiled stellar masses were re-scaled to a Baldry & Glazebrook (2003) IMF. However, the stellar masses of our study were derived by Mendel14 using mass-to-light (M/L) ratios for a Chabrier IMF. In order to carry out a consistent comparison, we have converted Damjanov et al. (2011) stellar mass values into the Chabrier IMF counterparts. The M/L conversion follows the prescriptions presented by Bernardi et al. (2010, table 2), where masses with Chabrier IMF are 0.055 dex heavier than those estimated with a Baldry & Glazebrook IMF. Effective radii are circularized, as in equation (1), and converted into physical sizes. The velocity dispersion measurements were extracted from the original studies and corrected to a common aperture of one effective radius, using the prescription of Cappellari et al. (2006).

Traditionally, red nuggets have been loosely defined as high-redshift ($z \sim 1.5$) quiescent galaxies with high masses $M_{\star} \sim 10^{11}\,\mathrm{M}_{\odot}$ yet small effective radii $R_{\mathrm{e}} \sim 1$ kpc. In order to avoid any ambiguity introduced by a free interpretation of the above definition, we have imposed tight constraints on the sample selection based on the vDokkum15 compactness criterion (equation 3).

Table 2 summarizes the different studies contributing to our red nugget sample. Column 3 shows the number of objects in each sample, followed by the number of galaxies with measured velocity dispersion, σ, in parentheses. The numbers of galaxies identified as compact (vDokkum15) are shown in the fourth column. In summary, the final sample contains 534 red nuggets (see Fig. 2), 218 of them with velocity dispersion measurements.

The less strict Barro13 compactness criterion (equation 2), with its lower mass limit, would generate a larger sample of 769 red nuggets, but at the cost of contaminating the sample with star-forming galaxies. In a study of star-forming galaxy contamination of assumed quiescent galaxy samples, Moresco et al. (2013) find that, for $z > 0.5$ and $\log(M_{\star}/\mathrm{M}_{\odot}) < 10.25$, up to 85 per cent of the galaxies show high specific star formation rates (sSFR), i.e. $\log(\mathrm{sSFR}/\mathrm{Gyr}^{-1}) > -2$. The precise percentage depends on

Table 2. Data compilation for the red nugget sample. The second column shows the redshift range of each contribution, with the number of objects displayed in the two last columns. The third column shows the total number of objects from each contribution, followed by the number of objects with measured velocity dispersion, σ, in parentheses. With a similar format, the last column shows the number of objects satisfying the vDokkum15 compactness criterion.

Contributions	Redshift	Objects	
		Total (σ)	Compact
Damjanov et al. (2011) compilation			
Saglia et al. (2010)	0.24–0.96	154 (154)	70 (70)
Schade et al. (1999)	0.29–0.99	36 (0)	3 (0)
Treu et al. (2005)	0.18–1.14	76 (76)	30 (30)
Rettura et al. (2010)	1.09–1.35	44 (0)	17 (0)
Newman et al. (2010)	1.05–1.59	17 (17)	7 (7)
McGrath, Stockton & Canalizo (2007)	1.29–1.59	5 (0)	3 (0)
Longhetti et al. (2007)	1.22–1.70	9 (0)	9 (0)
Ryan et al. (2012)	1.33–1.62	6 (0)	2 (0)
Damjanov et al. (2011)	0.62–1.75	31 (0)	10 (0)
Carrasco, Conselice & Trujillo (2010)	1.23–1.36	3 (0)	3 (0)
Damjanov et al. (2009)	1.40–1.85	10 (0)	7 (0)
Saracco, Longhetti & Gargiulo (2011)	0.96–1.91	15 (0)	1 (0)
Cassata et al. (2010)	1.32–1.98	4 (0)	1 (0)
Cimatti et al. (2008)	1.42–1.98	8 (0)	5 (0)
Daddi et al. (2005)	1.39–2.67	6 (0)	4 (0)
van Dokkum et al. (2008)	2.02–2.56	9 (0)	9 (0)
van de Sande et al. (2013) compilation			
van de Sande et al. (2013)	1.46–2.09	5 (5)	5 (5)
Bezanson et al. (2013)	1.24–1.62	6 (6)	5 (5)
van Dokkum, Kriek & Franx (2009)	2.19	1 (1)	1 (1)
Onodera et al. (2012)	1.43–1.83	18 (1)	11 (1)
Cappellari et al. (2009)	1.42	2 (2)	0 (0)
van der Wel et al. (2008)	0.83–1.14	40 (40)	14 (14)
Toft et al. (2012)	1.80–2.19	1 (1)	1 (1)
Others			
Trujillo et al. (2007)	0.42–1.89	421 (0)	227 (0)
Krogager et al. (2014)	1.84–2.20	14 (0)	5 (0)
Belli et al. (2014b)	0.90–1.58	11 (11)	11 (11)
Belli, Newman & Ellis (2014a)	2.09–2.43	5 (5)	5 (5)
Bezanson, Franx & van Dokkum (2015)	0.36–1.03	103 (103)	2 (2)
Zahid et al. (2015)	0.21–0.75	150 (150)	66 (66)
Total	0.18–2.67	1239 (601)	534 (218)

the quiescence selection criterion. Conversely, for $\log(M_\star/\mathrm{M}_\odot) > 10.75$, the contamination decreases to 30 per cent. From Moresco et al. (2013, fig. 10 and table 2), we can conclude that any quiescent galaxy sample with a cutoff at $\log(M_\star) \geq 10.6$ will be significantly cleaner than its analogue with $\log(M_\star) \geq 10.0$. In summary, unless stated differently (e.g. in the number density comparison, Section 3.3), our red nugget sample follows the vDokkum15 compactness criterion.

3 RESULTS

3.1 Photometric structural comparison

The question we pose here is: are there red nugget-like cores at $z \sim 0.1$?

A considerable number of the $z \sim 0.1$ galaxy cores in our sample are found to be structurally similar to the red nuggets. Specifically, 10 566 compact cores satisfy the vDokkum15 criterion, and thus share the same mass–size region as the red nuggets, as shown in Fig. 1.

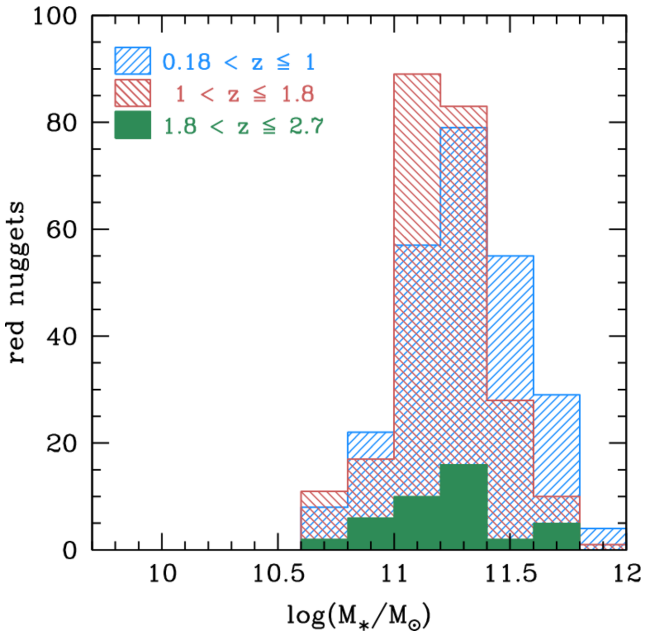

Figure 2. Histogram of the 534 red nuggets that fulfil the vDokkum15 compactness criterion, separated into three redshift bins and shown as a function of their stellar mass.

In Fig. 3, built on the spheroidal family portrait by Graham (2013, fig. 1), we put compact cores and red nuggets in the context of the other known members of the spheroidal family, including globular clusters, ultra-compact dwarfs (UCD), compact ellipticals (cE), dwarf spheroidals, dwarf ellipticals (dE) and normal ellipticals (E). The right-hand plots of Fig. 3 zoom on the selected portrait regions where data from the present study are concentrated.

Mass–size and mass–density relations are presented in Fig. 3. Stellar masses are computed either for each galaxy as a whole, in the case of ellipticals and red nuggets, or for compact cores as individual structures. The stellar mass density $\rho_{1/2}$ has been defined within the volume containing half each object's light. We take the half-light volume radius to be $r_{1/2} \sim 4/3 \times R_\mathrm{e}$. This relation between the 2D projected effective radius R_e and the 3D half-light radius ($r_{1/2}$) is shown to be valid for most surface brightness profiles and a wide range of Sérsic indices (Ciotti 1999; Wolf et al. 2010):

$$\rho_{1/2} \equiv \frac{3M_\star}{8\pi r_{1/2}^3} \approx \frac{0.05M_\star}{R_\mathrm{e}^3}. \quad (5)$$

For the density computation, we assume that the M/L ratio within the cores is constant with radius; therefore, half of the stellar mass of the core is enclosed inside the half-light radius ($r_{1/2}$). For reference, the figures include the mass–size and mass–density relations form Shen et al. (2003). Their original relation, $\log(R_\mathrm{e}/\mathrm{pc}) = 0.56\log(M_\star/\mathrm{M}_\odot) - 2.54$, has been converted from Kroupa (2001) IMF to Chabrier IMF, by adding 0.05 to the right-hand side of the equation (Bernardi et al. 2010, table 2). As expected, there is a good match between this relation and our reference ellipticals. The slight discrepancy – a steeper mass–size relation at higher masses and a flatter one for lower masses – has been explained by Mosleh, Williams & Franx (2013) in terms of biased size measurements originating from the adopted fitting law (see also Appendix B). Also La Barbera et al. (2010) reported systematically lower effective radii for luminous SDSS galaxies due to sky overestimation.

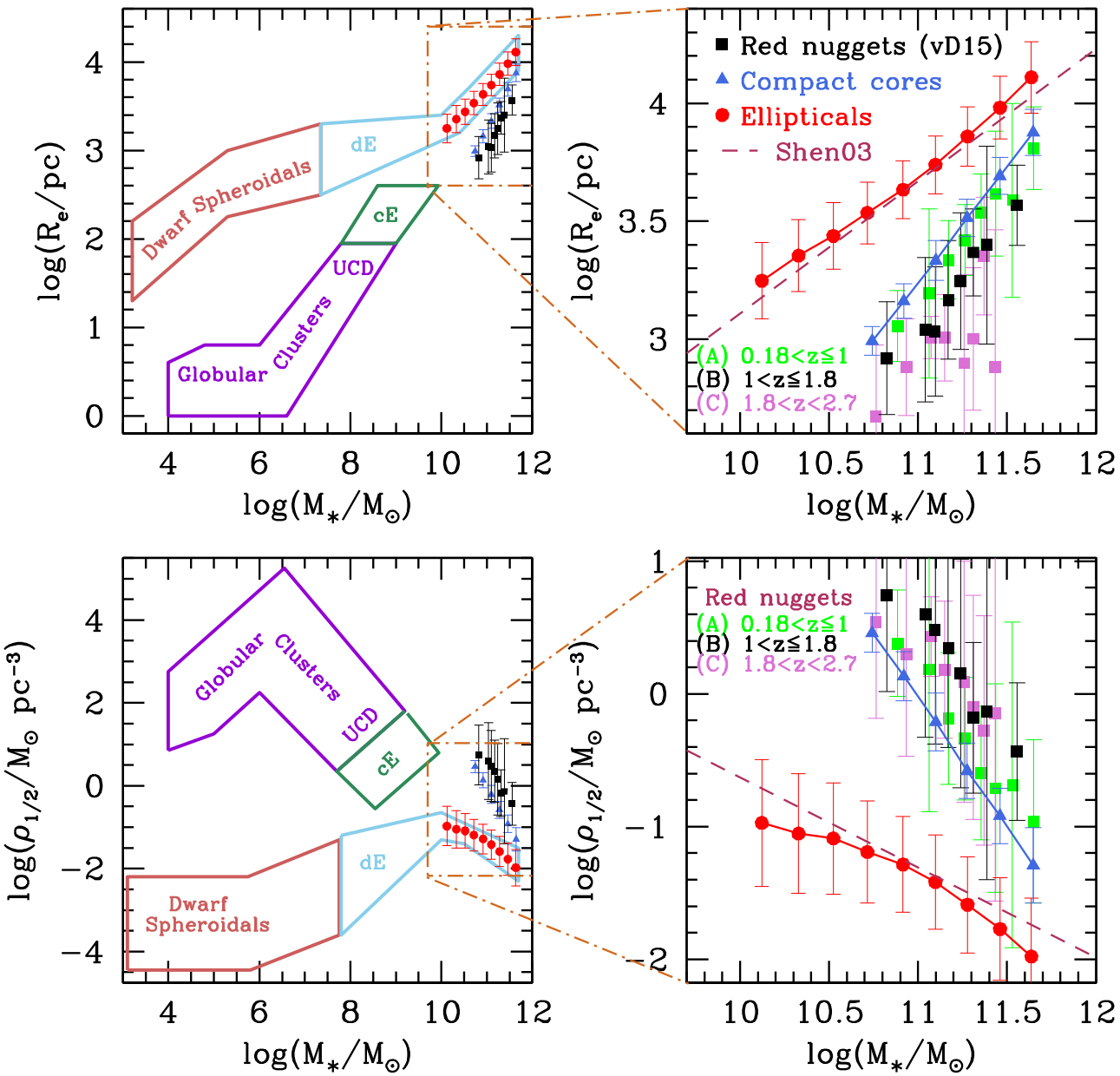

Figure 3. The place of compact cores and red nuggets in the spheroidal family map. The upper-left panel shows the general mass–size plane, including dwarf spheroidals, dwarf ellipticals (dE), normal ellipticals, globular clusters, ultra-compact dwarfs (UCD), compact ellipticals (cE). In the upper-right panel, an amplification of our main contribution is shown. Median values of our elliptical galaxies match the results from Shen et al. (2003) and segregate from the compact cores and red nuggets. The red nugget sample has been divided into three redshift slices, whose mass–size relations approach compact cores as redshifts gradually decrease. The lower half of the figure shows the mass–density relation with a similar format.

Median values and rms dispersion (compact cores and ellipticals) have been computed for stellar mass bins with equal width of 0.2 dex, excluding bins with less than 60 objects. For the red nugget subsample, median values and dispersion were calculated in eight equal-sized bins. The red nugget sample has been subdivided into three redshift slices, (bin A) $0.18<z\leq1$; (bin B) $1<z\leq1.8$ and (bin C) $1.8<z<2.7$, the first two with comparable sizes (254 and 239) and the third one with just 41 elements.

Mass–size relations in the upper part of Fig. 3 show that, for galaxies of similar mass, compact cores and red nuggets are two to five times smaller than ellipticals, showing also a different slope, α ($R_{\rm e}\propto M_{\star}^{\alpha}$). On one side, the ellipticals (also Shen et al. 2003) have $\alpha=0.56$. On the other side, compact cores, bin A and bin B red nuggets have $\alpha=0.98$, 0.96 and 0.95, respectively. Note that the values of these slopes are a consequence of the selected compactness criterion. For instance, the reported $\langle\alpha\rangle\sim0.96$ values are driven by our choice of the vDokkum15 compactness criterion (equation 3), where $\alpha=1$.

The redshift evolution of the intercept in the mass–size relation, i.e. the change in average size at a given stellar mass, has been parametrized by Trujillo et al. (2006b) as $\langle R_{\rm e}\rangle_{M_{\star}}\propto(1+z)^{\beta}$. Values of the order of $\beta\sim-1.5$ have been reported for massive Early Type Galaxies (ETGs) in general (Newman et al. 2012; vdWel14). In the frame of our hypothesis, where we compare red nuggets with $z\sim0.1$ compact cores, the mass–size trends of both samples will by definition be very similar, both being subject to the same mass–size

selection limits. We therefore find a much smaller effective $\beta \approx -0.7$. For instance, the average size of red nuggets at $\log(M_\star/\mathrm{M}_\odot) = 11$ changes from just 1 to 1.4 kpc from $z \sim 1.4$ to 0.6, and the average size of compact cores at this mass at $z \sim 0.1$ is just 1.7 kpc. So the mean size of the sub-population is relatively static, but slowly approaching its selection limit (2 kpc at this mass; see equation 3).

The bottom panels in Fig. 3 present the mass–density relation. Again, compact cores and red nuggets, selected with the same vDokkum15 criterion, are segregated from the reference ellipticals, showing significantly higher densities at a given mass. For instance, at $\log(M_\star/\mathrm{M}_\odot) = 11$, red nugget density $\log(\rho_{1/2}/\mathrm{M}_\odot\,\mathrm{pc}^{-3})$ decreases from 0.56 to 0.16 dex (i.e. 3.6 to 1.4 $\mathrm{M}_\odot\,\mathrm{pc}^{-3}$) from redshift bin B to A. There is an additional decrease to $\log(\rho_{1/2}/\mathrm{M}_\odot\,\mathrm{pc}^{-3}) \sim -0.02$ dex (i.e. to 0.95 $\mathrm{M}_\odot\,\mathrm{pc}^{-3}$) for $z \sim 0.1$ compact cores. This last density is more than 20 times larger than the typical one for elliptical galaxies of similar mass.

We have checked the robustness of our result against two possible sources of bias, i.e. the presence of AGN that can mimic a compact core in some galaxies, as well as the choice of a fixed Sérsic index $n_{\mathrm{bulge}} = 4$. As shown in Appendix B, these do not affect our results.

In summary, we have shown that a significant fraction of $z \sim 0.1$ galaxies contain compact cores structurally similar to red nuggets. The actual value of the fraction depends on the compactness criterion, but we find that 5 per cent of galaxies contain a core satisfying the most restrictive criterion applied here (vDokkum15).

3.2 Dynamical structural comparison

While stellar masses are dependent on assumptions about the stellar populations properties (e.g. age, metallicity and IMF), the dynamical masses follow more directly from observations of velocity dispersion and angular size. In this section, we will repeat the mass–size and mass–density relations in terms of dynamic mass measurements, comparing compact cores to red nuggets and elliptical galaxies. Velocity dispersion measurements in cores are vulnerable to light contamination from the disc/halo component, leading to artificially low values of σ_{core}. Our strategy to avoid core contamination uses stellar population measurements to single out disc light entering the spectroscopic fibre. As shown in Appendix C, we impose a cutoff at luminosity-weighted ages, $\langle\mathrm{Age}\rangle_{\mathrm{L}} \geq 9.05$ Gyr, to select 2548 uncontaminated compact cores. An aperture correction has been applied to bring velocity dispersion values to a common system, using Cappellari et al. (2006) prescription to convert each velocity dispersion into its equivalent at an aperture of one effective radius. Though such a prescription may not be accurate for cores, having been originally derived for luminous spheroids, the aperture corrections turn out to be very small, less than ∼2.2 per cent on average, implying that our results are not significantly affected by the method used to estimate the aperture corrections. As a further check, we have used an alternative prescription by Jørgensen, Franx & Kjaergaard (1995), giving nearly equal aperture-corrected values, with an insignificant mean offset of 1 km s^{-1}.

The first comparison involves the velocity dispersion (σ), the dynamical parameter one might presume to be less affected by the subtleties of photometric B+D decomposition. However, the measured σ are not exempt from some minor photometric dependences. First, the disc-contamination cutoff is based on the stellar mass ($M_\star$). Secondly, the σ aperture correction is derived from the core angular half-light radius and, thirdly, cores are binned according to their

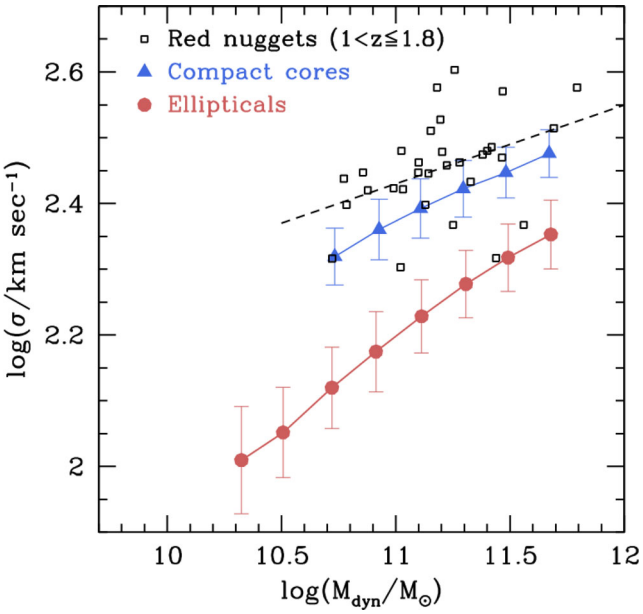

Figure 4. Median values of velocity dispersions (σ) for dynamical mass bins. Samples are compact cores (blue filled triangles), and reference elliptical galaxies (red filled dots). Due to the small sample size, the red nuggets in $1 < z \leq 1.8$ are represented as individual points (black open squares) with a linear fit shown as a dashed line.

dynamical mass, which depends on the effective radius. Dynamical masses are computed with the formula

$$M_{\mathrm{dyn}} = K\frac{\sigma_{\mathrm{e}}^2 R_{\mathrm{e}}}{\mathrm{G}} \tag{6}$$

with a fixed virial constant $K = 5$ deduced by Cappellari et al. (2006) for the ETGs.

In Fig. 4, we show the σ comparison between three different samples. First, 2548 compact cores selected according to the vDokkum15 compactness criterion and filtered for disc light contamination, as explained in Appendix C. Secondly, the reference elliptical galaxies defined in Section 2.2.2 also filtered for light contamination from young stellar populations (8090 objects) and thirdly, the 28 red nuggets in the redshift slice $1 < z \leq 1.8$, with available σ observation and $M_{\mathrm{dyn}} > M_\star$. From Fig. 4, we can deduce that compact cores and red nuggets are clearly segregated from normal ellipticals.

The mass–density relation is presented in Fig. 5 with median values of compact cores (blue filled triangles) and elliptical galaxies (red filled dots). Again, the small red nugget sample (28) is represented by individual black squares and a corresponding linear fit dashed line. Once again, the relative match between the compact cores and red nuggets should not come as a surprise, but as a natural consequence of sharing the same compactness criterion. In fact, vDokkum15 show that their compactness criterion corresponds to $\log(\sigma_{\mathrm{predicted}}/\mathrm{km\,s}^{-1}) > 2.40$.

3.3 Number densities

In this section, we compare the abundance of red nuggets at $z \sim 1.5$ with that of $z \sim 0.1$ compact cores. In Section 2.2.1, we have emphasized the sensitivity of the number density to the choice of a compactness criterion and the probed mass range; consequently, any number density comparison must be carried out based on given compactness and mass-selection criteria. We carry out a detailed

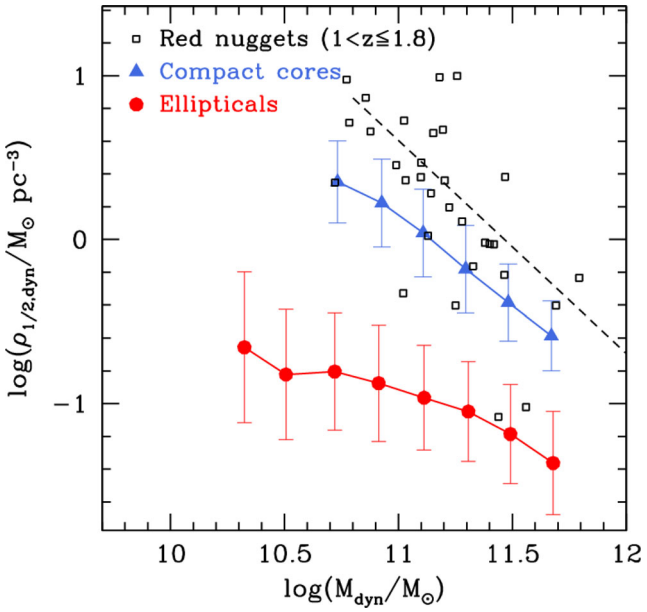

Figure 5. The dynamical version of the photometric mass–density relation in Fig. 3 is shown for individual red nuggets (black open squares), median values of compact cores (blue filled triangles) and reference elliptical galaxies (red filled dots). The dashed line corresponds to the linear fit to the red nuggets. There is a significant segregation of elliptical galaxies with respect to red nuggets and compact cores.

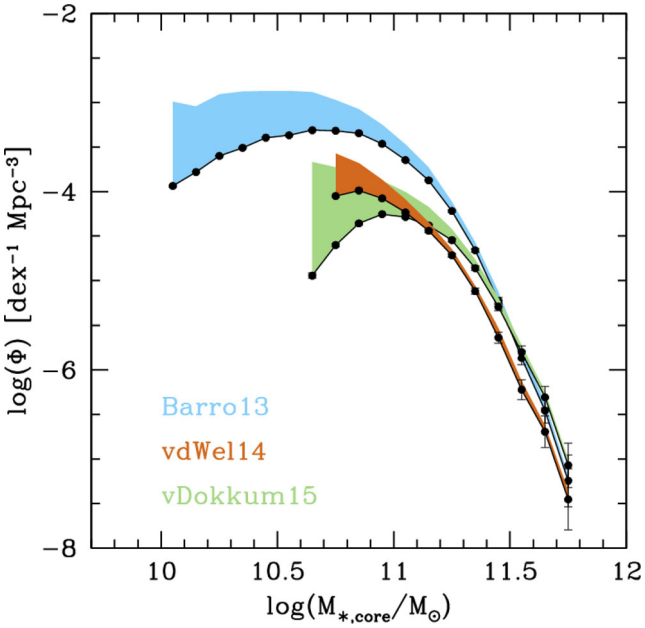

Figure 6. Compact core mass function for the three alternative Barro13, vdWel14 and vDokkum15 compactness criteria. Each function spans the range between the upper and lower sample limits, as defined in the text. The lower mass cuts are tied to each compactness criteria definition.

comparison, by taking advantage of the three available studies on the evolution with redshift of the red nugget abundance (Barro13; vdWel14; vDokkum15).

We make use of the three compact core samples defined in Section 2.2.1 and Table 1 in the 8032 deg^2 area coverage of the SDSS-DR7 Legacy Survey (Abazajian et al. 2009). Compact core mass functions (CMFs) have been computed for each compactness criterion and shown in Fig. 6. As stated in Appendix A, $V/V_{\rm max}$ volume corrections are applied to account for any residual incompleteness in our samples. Our $V_{\rm max}$ calculation follows similar procedures as in Simard11 and Shen et al. (2003), and mass functions (MFs) are calculated for the redshift range $0.025 \leq z \leq 0.15$. Differences among the three MFs can be understood based on the compactness criteria illustrated in Fig. 1, where one can see, for instance, that the vDokkum15 criteria are more restrictive, at all but at high masses, than those of Barro13 and vdWel14. As mentioned in Section 2.2.1, the selections in Table 1 provide lower limits for the number density. We have worked out corresponding upper limits by reinstating some systems that were excluded when creating the pure sample (due to disc inclination, core elongation, image resolution or Type-4 anomalous decomposition). For instance, filtering by core elongation will exclude genuine compact cores coexisting with bars. The final numbers of compact cores in the upper limit samples are 153 038 for Barro13, 25 426 for vdWel14 and 21 830 for vDokkum15 criteria. Fig. 6 displays the three MFs represented as a band enclosed between the upper and lower limit MFs (black connected dots).

The lower and upper number density limits can be compared with those for red nuggets, at different redshifts. Filled dots with error bars in Fig. 7 are extracted from the published plots in Barro13 (fig. 5), vdWel14 (fig. 13) and vDokkum15 (fig. 19). Dark shaded horizontal bands in Fig. 7 correspond to the upper and lower limit compact core number density at $z \sim 0.1$, stretched along the width of the plot to aid the comparison with the red nuggets. These values correspond to the integral of the upper and lower limits of the MFs in Fig. 6. Results are also reported in Table 3.

Table 3. Upper and lower number density limits (column 3) for galaxy cores with different compactness criteria and mass ranges. Maximum number densities for red nuggets (column 4) have been extracted from the literature.

Compactness criteria		Number density	
Reference	Mass range	Compact cores lower–upper limits	Red nuggets maximum
	$\log(M_{\star,\,\rm core}/{\rm M}_\odot)$	(10^{-4} Mpc^{-3})	(10^{-4} Mpc^{-3})
Barro13	≥ 10.00	1.73–3.12	2.4 ± 1.0
vdWel14	≥ 10.70	0.40–0.78	1.7 ± 0.2
vDokkum15	≥ 10.60	0.28–0.72	1.4 ± 0.1

Fig. 7 also plots the number density of the bona fide ellipticals at $z \sim 0.1$ that satisfy, as a whole, the compactness criteria (see dashed shaded region), as well as the number density of $z \sim 0.1$ compact cores residing only in ellipticals (with respect to other galaxy types). The density of compact ellipticals is further discussed in Section 4. The low abundance of ellipticals hosting a compact core, with respect to the number density of red nuggets, would refute any proposal that the centre of present-day ellipticals may be the only evolutionary path for red nuggets.

From Fig. 7 we can conclude that the $z \sim 0.1$ compact core number density is comparable to that of red nuggets. In agreement with our results, recent cosmological hydrodynamical simulations on the evolution of red nuggets (Furlong et al. 2015; Wellons et al. 2016) conclude that only a fraction of them have survived by $z \sim 0$. For instance, Wellons et al. (2016) find that 'about half acquire an *ex situ* envelope and exist as the core of a more massive descendant, 30 per cent survive undisturbed and gain very little mass...'.

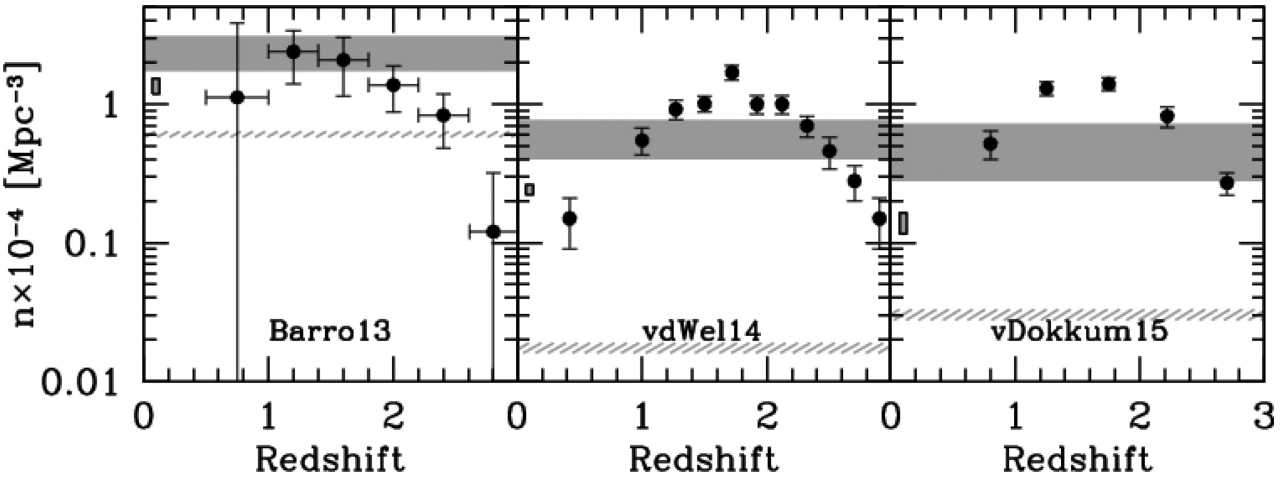

Figure 7. Evolution with redshift of the number density of massive quiescent compact galaxies for the three alternative compactness criteria. The filled dots with error bars are extracted from fig. 5 of Barro13, fig. 13 of vdWel14 and fig. 19 of vDokkum15. Our compact core number density results are represented by a shaded dark grey band confined between the upper and lower limits discussed in the text. Although our result corresponds to redshift ∼0.1, the band is stretched along the full redshift range to aid the comparison with the high-redshift data. The figure also plots the number density of elliptical galaxies hosting a compact core, shown as a small shaded rectangle at redshift ∼0.1. Secondly, the number density of entire galaxies, at $z \sim 0.1$, satisfying the compactness criterion, is shown as a dashed shaded band.

Table 4. Morphology class of galaxies hosting a compact core (vDokkum15). The class is assigned according to the definitions in column 2 (Meert et al. 2015). Morphology fractions are given for the sample in Table 1 (10 566 galaxies) and integrated for $\log(M_{\star,\,\mathrm{gal}}/\mathrm{M}_{\odot}) \geq 10.50$–$10.75$ bin.

Class	Definition	vDokkum15
Elliptical	T-type ≤ -3	50.9 per cent
S0	−3 < T-type ≤ 0.5	43.4 per cent
Sab	0.5 < T-type ≤ 4	5.4 per cent
Scd	4 < T-type	0.3 per cent

3.4 Morphology

The morphological class of the galaxies hosting compact cores contains information relevant to our study. The Huertas-Company et al. (2011) catalogue provides the automated morphological classification of the SDSS-DR7 spectroscopic sample, giving the probability P(E), P(S0), P(Sab) and P(Scd) of each galaxy type. These probabilities can be converted into the T-type classification scheme of Nair & Abraham (2010) with the simple linear model computed by Meert et al. (2015),

$$\text{T-type} = -4.6P(\text{E}) - 2.4P(\text{S0}) + 2.5P(\text{Sab}) + 6.1P(\text{Scd}). \quad (7)$$

We also follow Meert et al. (2015, equation 8) in the definition of the galaxy morphology classes in terms of T-type, which is presented in the second column of Table 4.

Our goal here is to assess the morphological variety of the fully fledged galaxies that host compact cores (rather than analysing the compact core structure itself as in Section 3.1). Fig. 8 and Table 4 show these results, with mass estimates, $M_{\star,\,\mathrm{gal}}$, also being for the total host galaxy (not the core mass).

Fig. 8 shows the variation along $M_{\star,\,\mathrm{gal}}$ of the four morphology class fractions. Aside from the Scd class, which contributes a negligible amount, the other classes are identified by coloured bands. Inside each colour band, lines and symbols identify the results of each compactness criterion. Only the Barro13 results span the mass range down to the $\log(M_{\star,\,\mathrm{gal}}) \sim 10$ level. The histograms, in the lower part, show the mass range covered by each compactness criterion. Note that very few galaxies, hosting compact cores, populate the $\log(M_{\star,\,\mathrm{gal}}/\mathrm{M}_{\odot}) = 10.50$–$10.75$ bin (19 galaxies for vDokkum15 and 40 for vdWel14) and their presence is imperceptible in the histogram. Nevertheless, the morphology fraction is calculated for those galaxies.

Table 4 gives for morphology fractions integrated across all masses (hence less detailed than the mass-dependent results shown in Fig. 8). Using the vDokkum15 sample in Table 1, all host galaxies with compact cores of $\log(M_{\star,\,\mathrm{core}}) \geq 10.6$ (10 566) are integrated into four morphology fraction values. Host galaxy morphology essentially divides into a 50:50 mixture of elliptical and disc morphology (note that the majority of the sample is in early-type systems: E + S0). An alternative option to Fig. 8, using $M_{\star,\,\mathrm{core}}$ masses, is considered in Appendix D.

According to Fig. 8, S0 and Sab classes dominate the morphologies of galaxies hosting compact cores, for $\log(M_{\star,\,\mathrm{gal}}) \leq 11.0$. At the high-mass end, elliptical galaxies predominate over their disc counterparts. Integrated values in Table 4 give more balanced results with comparable fractions of elliptical and S0 classes and minor contributions from later-type disc classes.

A further simple computation can provide an estimation of the average extra stellar mass incorporated on top of the naked red nuggets to become fully fledged present-day galaxies. Assuming that the red nuggets survive intact since redshift ∼1.5, the extra mass acquired during the last ∼9.2 Gyr equates to the difference between the total and the core masses, roughly equal to the B+D decomposed disc mass (M_{d}) in Mendel14. The average extra mass for the vDokkum15 selected sample is $\log(M_{\star,\,\mathrm{extra}}/\mathrm{M}_{\odot}) = 10.53$, which means that an average 25.3±13.5 per cent of the total galaxy mass at $z \sim 0.1$ has been accreted since $z \sim 1.5$ at a growth rate $\sim 3.7\,\mathrm{M}_{\odot}\,\mathrm{yr}^{-1}$. These results are consistent with those of van Dokkum et al. (2010), who estimate that ∼40 per cent of the total stellar mass at $z = 0$ would have been added through mergers since $z \sim 2$ under this hypothesis. There is even better agreement with Patel et al. (2013), who report a 33 per cent mass increase from $z \sim 1.5$ to $z \sim 0.1$.

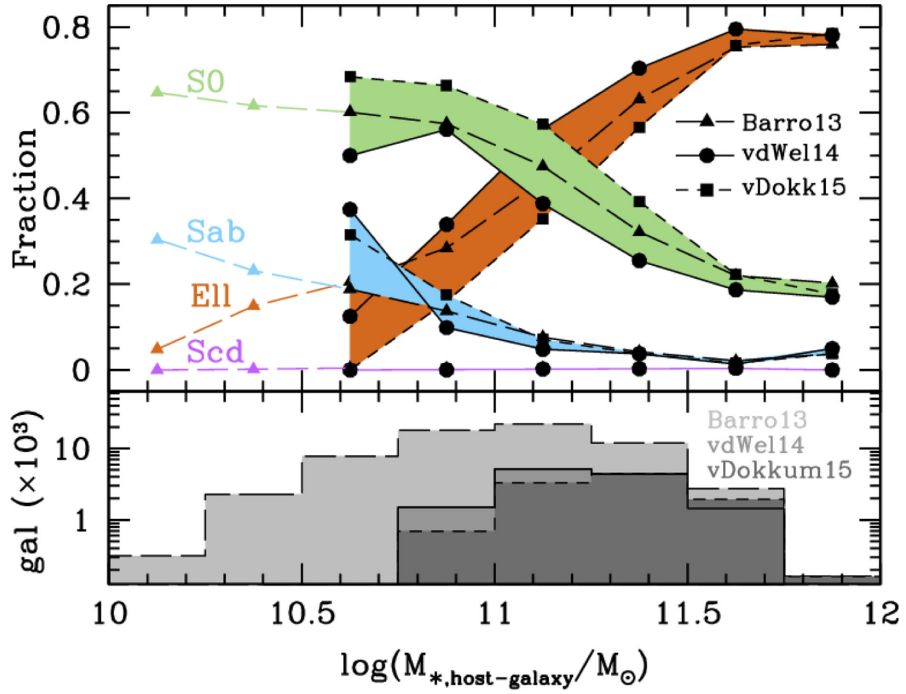

Figure 8. The morphology class fraction of galaxies hosting a compact core. Both mass and morphology correspond to the whole galaxies. In the upper panel, the results are presented for the three alternative criteria used to select the compact cores: Barro13 (triangles), vdWel14 (dots) and vDokkum15 (squares). Coloured bands correspond to each morphology class. The coloured triangle extensions correspond to the Barro13 criterion, which includes host galaxies down to $\log(M_{\star,\,\mathrm{gal}}/\mathrm{M}_{\odot}) \geq 10.0$. In the lower panel, three histograms are shown with the total stellar mass of the host galaxy, using a bin size 0.25 dex. It should be noted that very few host galaxies populate the 10.5–10.75 mass bin (19 for vDokkum15 and 40 for vdWel14), but nevertheless their morphology fractions have been calculated.

4 DISCUSSION

A few recent studies have offered interesting explanations for the early red nugget density evolution at redshifts larger than $z \sim 2$. Barro13 offer a convincing explanation for the number density increase of red nuggets earlier than $z \sim 2$, built on the simultaneous decline of the number density of sCMGs. Their result has been corroborated by vDokkum15. This interpretation suggests that the sCMGs are being continuously converted into red nuggets by processes quenching their star formation, while new sCMGs are replenished by cold flows, until that process becomes inefficient by $z \leq 1.5$. Oddly, red nugget evolution below $z \sim 1.5$ is characterized by observational disagreement and the lack of unanimous interpretation.

For instance, our relatively high number density of $z \sim 0.1$ compact cores $(0.28–0.72) \times 10^{-4}$ Mpc^{-3} (see Table 3 and Fig. 7) comes into apparent conflict with the majority of the results from the literature, which range from lower ($\sim 10^{-7}$ Mpc^{-3}; Trujillo et al. 2009; Taylor et al. 2010) to higher number densities ($\sim 10^{-5}$–10^{-4} Mpc^{-3}; Valentinuzzi et al. 2010; Poggianti et al. 2013). This conflict is only *apparent* because the discrepancy results from the adoption of different search strategies, looking for either compact full galaxies (literature) or compact cores (this study). Contrary to compact cores, which are relatively abundant, very few full galaxies satisfy the demanding compactness criteria in their own right. In order to check this statement, we have used our own data to calculate the number density of full galaxies satisfying the vDokkum15 compactness criterion. By using the single-Sérsic fit version of the mass–size parameters from the Mendel14 catalogue, we obtain a number density of 3.0×10^{-6} Mpc^{-3}, an order of magnitude lower than the corresponding compact core number density (as shown in Fig. 7).

According to the hypothesis we are testing here, red nuggets – once formed – do not significantly change their internal structure or composition, but simply aggregate 2D or 3D envelopes to become the compact massive cores of present-day galaxies. Under this hypothesis, the number density of $z \sim 0.1$ compact cores should approximately match, or be slightly less than, the maximum value attained by the red nuggets. We have now shown that this is the case (see Fig. 7 and Table 3). This result is in agreement with a recent study by Graham et al. (2015), their sample of 21 structurally decomposed lenticular galaxies also having a relatively high number density, comparable to our own lower limits. Comparison with full galaxies at $z \sim 0.1$, rather than with compact cores, leads to a discrepancy, as shown here and in the literature. This is in no conflict with the above hypothesis which asserts only that the cores are sufficient – not necessary – building blocks for $z \sim 0.1$ galaxies.

5 SUMMARY AND CONCLUSIONS

In this study, we have tested the hypothesis that high-redshift compact, quiescent and massive galaxies, nicknamed *red nuggets*, have survived as the compact cores of massive present-day elliptical or disc galaxies. Two main questions are posed to test this hypothesis:

(i) Do compact cores, structurally similar to red nuggets, exist at $z \sim 0.1$?

(ii) If so, is their abundance comparable to that of red nuggets at $z \sim 1.5$?

We carry out this test using the recently published SDSS-based large catalogues of bulge+disc (B+D) galaxy decompositions, in particular from Mendel14, which includes stellar masses of the B and D structural components. We approach the test from a comprehensive perspective, imposing the B+D decomposition to the whole present-day galaxy sample, regardless of their morphology types. We adopt the generic name *core* to include the central component of ellipticals and bulge of discs, and study these as if they were independent structures, defined based on their compactness, according to the same criteria adopted in the literature to identify the red nuggets themselves (e.g. vdWel14; Barro et al. 2015; vDokkum15). It is worth mentioning that our results depend heavily on the reliability of the photometric B+D decomposition of SDSS galaxy data. Nevertheless, the huge size of the parent catalogue has allowed us to carry out a very strict quality screening, only passed by ∼30 per cent of the objects.

In summary, the study concludes that the answer to both these questions above is *yes*. The details of this conclusion and other key results are as follows.

(i) We confirm that a small but significant fraction (>5 per cent) of cores in present-day galaxies (regardless of morphology) is structurally similar to $z \sim 1.5$ red nuggets. In the mass–size and mass–density relations, the red nuggets and compact cores are significantly segregated from the normal elliptical galaxies, with average sizes ∼4 times smaller and densities ∼20 times larger than normal ellipticals at a given mass (e.g. $M_\star \sim 10^{11}\mathrm{M}_\odot$) (Fig. 3).

(ii) Not only do such compact cores exist, but their abundance matches approximately that of the red nuggets at $z \sim 1.5$ (e.g. vDokkum15). This result is quite consistent with previous findings on the present-day abundance of compact galaxies, as we use of B+D decomposed cores (rather than to full galaxies).

(iii) That these number densities are, if anything, slightly lower than the highest values for red nuggets further agrees with the hypothesis, leaving room for the some ∼20 per cent of red nuggets to have been destroyed in major merger events (as found in some cosmological simulations; e.g. Wellons et al. 2016; Furlong et al. 2015).

(iv) Dynamical measurements of the samples of red nuggets, compact core and ellipticals corroborate the photometric analysis. Velocity dispersion, σ, and dynamical mass density in red nuggets and compact cores are systematically larger than in normal ellipticals. For instance at a given $M_{\rm dyn} = 10^{11}\,\mathrm{M}_\odot$, σ is 1.5–1.7 times larger and dynamical mass density 11–35 times higher than in the normal ellipticals (Figs 4 and 5).

(v) A simple calculation allows us to estimate the extra mass accreted by the red nuggets to become fully fledged galaxies, under this hypothesis. Assuming that red nuggets start 'naked' or with only rudimentary discs at $z \sim 1.5$, the extra stellar mass acquired over the last ∼9 Gyr is the difference between the mass of the galaxy and that of the compact core. We find that galaxies hosting a compact core would typically have accreted one quarter of their mass over the last ∼9 Gyr, at a growth rate of $\sim 3.7\,\mathrm{M}_\odot\,\mathrm{yr}^{-1}$.

(vi) Galaxies hosting compact cores (according to the vDokkum15 criterion) show varied morphological classes extending from ellipticals to spirals (Scd). The integrated fractions of morphology classes with $\log(M_{\rm gal}/\mathrm{M}_\odot) > 10.5$ are 50.9 per cent (E), 43.4 per cent (S0), 5.4 per cent (Sab) and 0.3 per cent (Scd). Results for alternative mass ranges and compactness criteria are given in Fig. 8 and Appendix D. These findings are consistent with red nuggets becoming cores of both present-day elliptical and disc galaxies.

ACKNOWLEDGEMENTS

We thank the referee for a very constructive report, which improved the paper. We also thank Ignacio Trujillo, María Cebrián and the Galaxy Group at the IAC for enlightening discussions. We acknowledge the use of SDSS data (http://www.sdss.org/collaboration/credits.html), and support from grants AYA2013-48226-C3-1-P and AYA2013-47742-C04-02-P from the Spanish Ministry of Economy and Competitiveness (MINECO). IF thanks the IAC for hospitality under the Severo Ochoa visitor programme. MS and CdV acknowledge financial support from the MINECO under the 2011 Severo Ochoa Program SEV-2011-0187. CdV, MS and IM-V acknowledge financial support from MINECO under grants AYA2013-46886-P and AYA2014-58308-P.

REFERENCES

Abazajian K. N. et al., 2009, ApJS, 182, 543
Baldry I. K., Glazebrook K., 2003, ApJ, 593, 258
Baldwin J. A., Phillips M. M., Terlevich R., 1981, PASP, 93, 5
Barro G. et al., 2013, ApJ, 765, 104 (Barro13)
Barro G. et al., 2015, ApJ, Submitted, preprint (arXiv:1503.07164)
Belli S., Newman A. B., Ellis R. S., 2014a, ApJ, 783, 117
Belli S., Newman A. B., Ellis R. S., Konidaris N. P., 2014b, ApJ, 788, L29
Berg T. A. M., Simard L., Mendel T. J., Ellison S. L., 2014, MNRAS, 440, L66
Bernardi M., Shankar F., Hyde J. B., Mei S., Marulli F., Sheth R. K., 2010, MNRAS, 404, 2087
Bezanson R., van Dokkum P. G., Tal T., Marchesini D., Kriek M., Franx M., Coppi P., 2009, ApJ, 697, 1290
Bezanson R., van Dokkum P., van de Sande J., Franx M., Kriek M., 2013, ApJ, 764, L8
Bezanson R., Franx M., van Dokkum P., 2015, ApJ, 799, 148
Bluck A. F. L., Mendel J. T., Ellison S. L., Moreno J., Simard L., Patton D. R., Starkenburg E., 2014, MNRAS, 441, 599
Buitrago F., Trujillo I., Conselice C. J., Häussler B., 2013, MNRAS, 428, 1460
Cappellari M. et al., 2006, MNRAS, 366, 1126
Cappellari M. et al., 2009, ApJ, 704, L34
Cardelli J. A., Clayton G. C., Mathis J. S., 1989, ApJ, 345, 245
Carrasco E. R., Conselice C. J., Trujillo I., 2010, MNRAS, 405, 2253
Cassata P. et al., 2010, ApJ, 714, L79
Chabrier G., 2003, ApJ, 586, L133
Cid Fernandes R., Mateus A., Sodré L., Stasinska G., Gomes J. M., 2005, MNRAS, 358, 363
Cimatti A. et al., 2008, A&A, 482, 21
Ciotti L., 1999, A&A, 249, 99
Conroy C., Gunn J. E., White M., 2009, ApJ, 699, 486
Côté P. et al., 2006, ApJS, 165, 57
Daddi E. et al., 2005, ApJ, 626, 680
Damjanov I. et al., 2009, ApJ, 695, 101
Damjanov I. et al., 2011, ApJ, 739, L44
Damjanov I., Geller M. J., Zahid H. J., Hwang H. S., 2015, ApJ, 806, 158
Dekel A. et al., 2009, Nature, 457, 451
Di Matteo P. et al., 2015, A&A, 577, A1
Dullo B., Graham A. W., 2013, ApJ, 768, 36
Fan L., Lapi A., De Zotti G., Danese L., 2008, ApJ, 689, L101
Ferreras I. et al., 2014, MNRAS, 444, 906
Furlong M. et al., 2015, preprint (arXiv:1510.05645)
Gadotti D. A., 2008, MNRAS, 384, 420
Graham A. W., 2013, in Oswalt T. D., Keel W. C., eds, Planets, Stars and Stellar Systems, Vol. 6. Springer-Verlag, Dordrecht, p. 91
Graham A. W., Worley C. C., 2008, MNRAS, 388, 1708
Graham A. W., Dullo B. T., Savorgnan G. A. D., 2015, ApJ, 804, 32
Hopkins P. F., Bundy K., Murray N., Quataert E., Lauer T. R., Ma C.-P., 2009, MNRAS, 398, 898
Huang S., Ho L. C., Peng C. Y., Li Z.-Y., Barth A. J., 2013, ApJ, 766, 47

Huertas-Company M., Aguerri J. A. L., Bernardi M., Mei S., Sanchez Almeida J., 2011, A&A, 525, 157
Johansson P. H., Naab T., Ostriker J. P., 2012, ApJ 754 115
Jørgensen I., Franx M., Kjaergaard P., 1995, MNRAS, 276, 1341
Kewley L. J., Dopita M. A., Sutherland R. S., Heisler C. A., Trevena J., 2001, ApJ, 556, 121
Krogager J.-K., Zirm A. W., Toft S., Man A., Brammer G., 2014, ApJ, 797, 17
Kroupa P., 2001, MNRAS, 322, 231
La Barbera F., de Carvalho R. R., de la Rosa I. G., Lopes P. A. A., Kohl-Moreira J. L., Capelato H. V., 2010, MNRAS, 408, 1313
Lackner C. N., Gunn J. E., 2012, MNRAS, 421, L2277
Lauer T. R. et al., 2007, ApJ, 664, 226
Licquia T. C., Newman J. A., 2015, ApJ, 806, 96
Loeb A., Peebles P. J. E., 2003, ApJ, 589, 29
Longhetti M. et al., 2007, MNRAS, 374, 614
McGrath E. J., Stockton A., Canalizo G., 2007, ApJ, 669, 241
Meert A., Vikram V., Bernardi M., 2015, MNRAS, 446, 3943
Mendel J. T., Simard L., Palmer M., Ellison S. L., Patton D. R., 2014, ApJS, 210, 3 (Mendel14)
Moresco M. et al., 2013, A&A, 558, 61
Morishita T., Ichikawa T., 2016, ApJ, 816, 97
Mosleh M., Williams R. J., Franx M., 2013, ApJ, 777, 117
Naab T., Johansson P. H., Ostriker J. P., Efstathiou G., 2007, ApJ, 658, 710
Naab T., Johansson P. H., Ostriker J., 2009, ApJ, 699, L178
Nair P. B., Abraham R. G., 2010, ApJS, 186, 427
Newman A. B., Ellis R. S., Treu T., Bundy K., 2010, ApJ, 717, L103
Newman A. B., Ellis R. S., Bundy K., Treu T., 2012, ApJ, 746, 162
Onodera M. et al., 2012, ApJ, 755, 26
Oser L., Ostriker J. P., Naab T., Johansson P. H., Burkert A., 2010, ApJ, 725, 2312
Patel S. G. et al., 2013, ApJ, 766, 15
Peth M. A. et al., 2015, MNRAS, Submitted, preprint (arXiv:1504.01751)
Poggianti B. M., Moretti A., Calvi R., D'Onofrio M., Valentinuzzi T., Fritz J., Renzini A., 2013, ApJ, 777, 125
Rettura A. et al., 2010, ApJ, 709, 512
Ryan R. E., Jr, et al., 2012, ApJ, 749, 53
Saglia R. P. et al., 2010, A&A, 524, A6
Sánchez-Blázquez P., 2016, in Laurikainen E., Peletier R., Gadotti D., eds, Astrophysics and Space Science Library, Vol. 418, Galactic Bulges. Springer International Publishing, Switzerland, p. 127
Saracco P., Longhetti M., Gargiulo A., 2011, MNRAS, 412, 2707
Saulder C., van den Bosch R. C. E., Mieske S., 2015, A&A, 578, 134
Schade D. et al., 1999, ApJ, 525, 31
Shen S., Mo H. J., Simon D. M., Blanton M. R., Kauffmann G., Voges W., Brinkmann J., Csabai I., 2003, MNRAS, 343, 978
Simard L., Mendel J. T., Patton D. R., Ellison S. L., McConnachie A. W., 2011, ApJS, 196, 11 (Simard11)
Strauss M. A. et al., 2002, AJ, 124, 1810
Tacchella S., Dekel A., Carollo C. M., Ceverino D., DeGraf C., Lapiner S., Mandelker N., Primack J. R., 2015, MNRAS, preprint (arXiv:1509.00017)
Taylor E. N., Franx M., Glazebrook K., Brinchmann J., van der Wel A., van Dokkum P. G., 2010, ApJ, 720, 723
Thomas D. et al., 2013, MNRAS, 431, 1383
Toft S., Gallazzi A., Zirm A., Wold M., Zibetti S., Grillo C., Man A., 2012, ApJ, 754, 3
Treu T. et al., 2005, ApJ, 633, 174
Trujillo I. et al., 2006a, MNRAS, 373, L36
Trujillo I. et al., 2006b, ApJ, 650, 18
Trujillo I., Conselice C. J., Bundy K., Cooper M. C., Eisenhardt P., Ellis R. S., 2007, MNRAS, 382, 109
Trujillo I., Cenarro A. J., de Lorenzo-Cáceres A., Vazdekis A., de la Rosa I. G., Cava A., 2009, ApJ, 692, L118
Trujillo I., Ferreras I., de la Rosa I. G., 2011, MNRAS, 415, 3903
Valentinuzzi T. et al., 2010, ApJ, 712, 226
van de Sande J. et al., 2013, ApJ, 771, 85
van der Wel A., Holden B. P., Zirm A. W., Franx M., Rettura A., Illingworth G. D., Ford H. C., 2008, ApJ, 688, 48
van der Wel A. et al., 2014, ApJ, 788, 28 (vdWel14)
van Dokkum P. G. et al., 2008, ApJ, 677, L5
van Dokkum P. G., Kriek M., Franx M., 2009, Nature, 460, 717
van Dokkum P. G. et al., 2010, ApJ, 709, 1018
van Dokkum P. G. et al., 2015, ApJ, 813, 23 (vDokkum15)
Vazdekis A., Sánchez-Blázquez P., Falcón-Barroso J., Cenarro A. J., Beasley M. A., Cardiel N., Gorgas J., Peletier R. F., 2010, MNRAS, 404, 1639
Wellons S. et al., 2016, MNRAS, 456, 1030
Wolf J., Martinez G. D., Bullock J. S., Kaplinghat M., Geha M., Muñoz R. R., Simon J. D., Avedo F. F., 2010, MNRAS, 406, 1220
Zahid H. J., Damjanov I., Geller M., Chilingarian I., 2015, ApJ, 806, 122
Zolotov A. et al., 2015, MNRAS, 450, 2327

APPENDIX A: SAMPLE COMPLETENESS

The Mendel14 parent sample spans a redshift range $0.005 \leq z \leq 0.4$ and covers magnitudes $14.0 \leq \mathrm{mag}_{\mathrm{Petro},\,r} \leq 17.77$, where the bright-end magnitude limit is set to avoid problematic deblending of luminous galaxies and the faint-end limit marks the completeness flux limit of the spectroscopic SDSS sample (Strauss et al. 2002). Rather than a flux-limited sample, we need a complete mass-limited one, given that the most relevant reference parameter of the present study is the core stellar mass ($M_{\star,\,\mathrm{core}}$). Although we use the V/V_{max} statistics to correct for residual incompleteness in number density estimations (Section 3.3), it is advisable to rely on a sample with the highest possible degree of completeness throughout our target mass range, $\log(M_{\mathrm{core}}/\mathrm{M}_{\odot}) \geq 10.0$.

To assess the sample completeness, we have worked out the CMF for redshift slices of $\Delta z = 0.025$ (see Fig. A1). To construct the CMF, we have used the Mendel14 decomposition parameter $\log M_{\mathrm{b}}$, corresponding to the logarithm of $M_{\star,\,\mathrm{core}}$, instead of the more common total stellar mass of the galaxy. The area coverage of the SDSS-DR7 Legacy Survey (Abazajian et al. 2009) is 8032 deg^2.

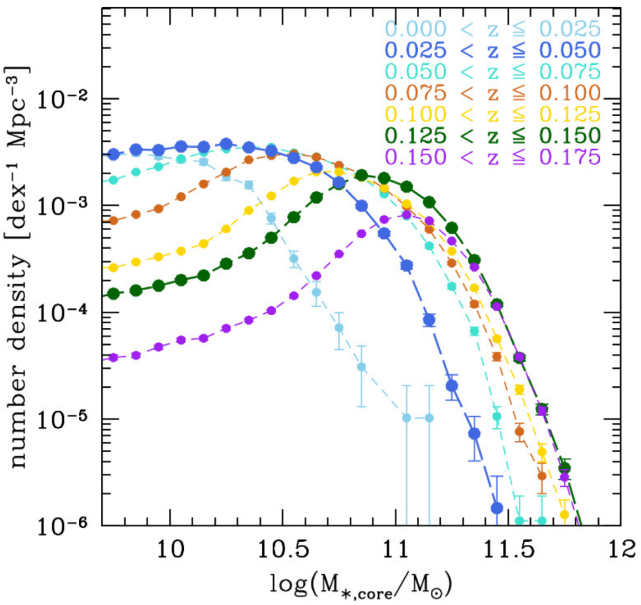

Figure A1. The CMF for redshift slices of $\Delta z = 0.025$ in the parent Mendel14 sample. Our strategy to obtain a nearly complete sample for $\log(M_{\mathrm{core}}/\mathrm{M}_{\odot}) \geq 10.0$ is based on avoiding redshift ranges which are poorly populated due to incompleteness. For instance, the $z \leq 0.025$ range is excluded due to high incompleteness at $\log(M_{\mathrm{core}}/\mathrm{M}_{\odot}) \geq 10.0$. The highest redshift bin is equally excluded and the selected redshift range for the sample is $0.025 \leq z \leq 0.150$.

As a first approximation, the upper envelope of all the curves is taken as our reference CMF. Our strategy to obtain a nearly complete sample for $\log(M_{\rm core}/{\rm M}_\odot) \geq 10.0$ is based on avoiding redshift ranges which are poorly populated due to incompleteness. The redshift range $0.025 \leq z \leq 0.150$ attains the highest completeness level for the $\log(M_{\rm core}/{\rm M}_\odot) \geq 10.0$ mass limit. The limiting CMFs for $0.025 \leq z \leq 0.15$ and $0.125 < z \leq 0.150$ are highlighted in Fig. A1 to enhance their contrast with the excluded neighbour redshift slices. The low-redshift slice $z \leq 0.025$ is rather incomplete at its high-mass end for $\log(M_{\rm core}/{\rm M}_\odot) \geq 10.0$, and the high-redshift slice $0.150 \leq z \leq 0.175$ is also very incomplete at its low-mass end.

APPENDIX B: POTENTIAL BIAS SOURCES

Two possible bias sources have been checked for their impact on the photometric B+D decompositions, namely the AGN emission and the choice of a fixed de Vaucouleurs shape for the compact cores.

In particular, the presence of strong emission from AGNs can bias our measurements of galaxy sizes towards small values. Following Thomas et al. (2013), we have extracted emission line fluxes to construct the BPT diagram (Baldwin, Phillips & Terlevich 1981). We designate an object as *emission* when the four diagnostic lines have been detected with signal-to-noise ratio above 2. The AGN identification in the BPT diagram follows the empirical separation from Kewley et al. (2001) and includes both the Seyfert and LINER classes. Galaxies designated as *emission* (AGN) make the 14 (5) per cent of the compact core subsample, while corresponding figures for the non-core elliptical subsample are 10 (4) per cent. The mass–size and mass–density relations (Fig. 3), represented by the median values in mass bins, are unaffected by the exclusion of AGNs or even the exclusion of *emission* objects, proving that AGN contamination is not an issue for our results.

Concerning the choice of the bulge Sérsic index, Mendel14 catalogue uses a fixed de Vaucouleurs bulge fit ($n_{\rm bulge} = 4$), instead of a free-$n_{\rm bulge}$ fit. According to the authors, the vast majority of SDSS images have insufficient spatial resolution and/or signal-to-noise ratio to provide an adequate $n_{\rm bulge}$ determination and there is no significant advantage on using free-$n_{\rm bulge}$ over fixed $n_{\rm bulge} = 4$ fits. As explained by Lackner & Gunn (2012), at the SDSS resolution, the bulges have their profile tail subsumed in the disc, while the central peak is washed out by the PSF, making a bulge with say $n_{\rm bulge} = 4$ indistinguishable from one with $3 \leq n_{\rm bulge} \leq 5$.

While Mendel14 only derive masses for the $n_{\rm bulge} = 4$ B+D fits, Simard11 provide photometric parameters for both free-n and fixed $n = 4$ fits. We have used our compact core sample (10 566 objects) to assess the potential bias introduced by the Sérsic index choice on the structural parameters.

Alternative galaxy/core size calculations are compared in Fig. B1. As a common base, we have used the total galaxy mass $\log(M_\star/{\rm M}_\odot)$ obtained from a single fit with a free-n Sérsic function. For $\log(M_{\star,\,\rm core}/{\rm M}_\odot) \geq 10.6$, free-$n$ cores are, on average, 0.11 $\pm$ 0.06 dex larger than $n = 4$ cores of similar mass. The use of free-n would decrease the reported separation of 0.38 $\pm$ 0.10 dex between the reference ellipticals and compact cores (see Section 3). As already mentioned, we avoided the use of free-n cores in the present study, due to the lack of $M_{\star,\,\rm core}$ information in the catalogues. In conclusion, the choice of Sérsic index does not drastically affect our results. The moderate sensitivity to the Sérsic index choice is an expected outcome of the distribution of the Sérsic indices in the free-n fits, which has 78 per cent of the values in the interval $3.5 \leq$ free-$n_{\rm bulge} \leq 7$, close to the fixed $n = 4$ value.

In Fig. B1, the behaviour of the lines representing the full-galaxy (green) and disc (purple) sizes can be explained in terms of the host galaxy morphology. The slight predominance of discs below $\log(M_\star/{\rm M}_\odot) \sim 11.3$ is seemingly related to the larger fraction of disc galaxies in the lower end of our mass interval (see Fig. 8). The prevalence of ellipticals at the high-mass end generates a drop in the disc sizes.

Fig. B2 represents alternative fits to the galaxies of the reference elliptical sample. As expected, the disc size is visibly smaller than the full galaxy and even the cores. Note that the cores of these

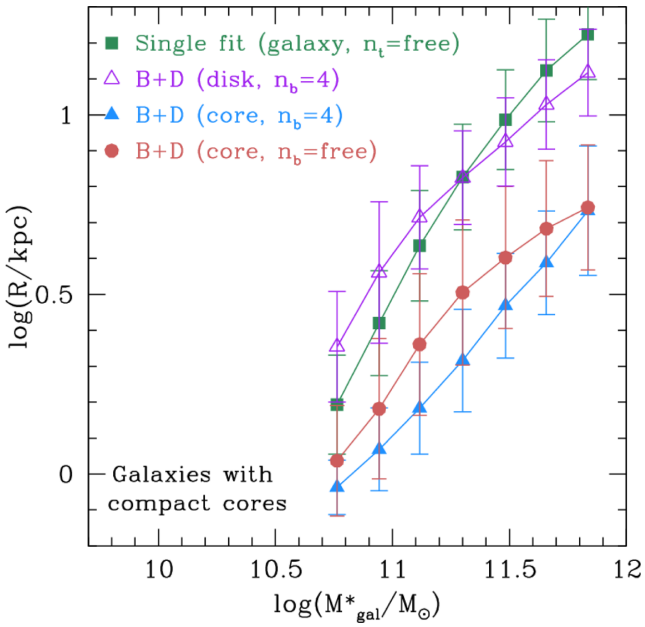

Figure B1. Variation of sizes determined with different fitting laws, for the compact core sample (10 566 objects), plotted as a function of total galaxy mass: galaxy effective radius measured with a single fit with a free-n Sérsic function (green squares); exponential disc scalelength measured with bulge+disc (B+D) decomposition with bulge Sérsic $n_{\rm b} = 4$ fit (open purple triangles); core effective radii calculated with $n_{\rm b} = 4$ (blue triangles) and $n_{\rm b}$ =free (red circles).

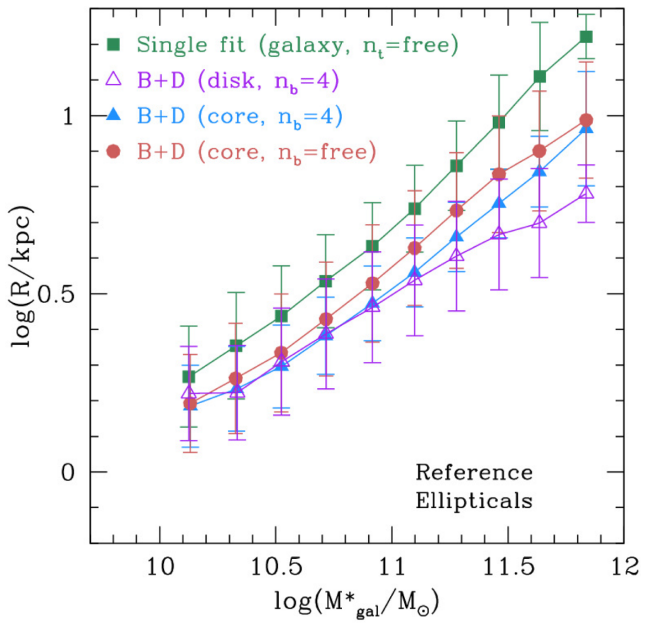

Figure B2. Same as Fig. B1, with equivalent symbols, but for the reference elliptical sample.

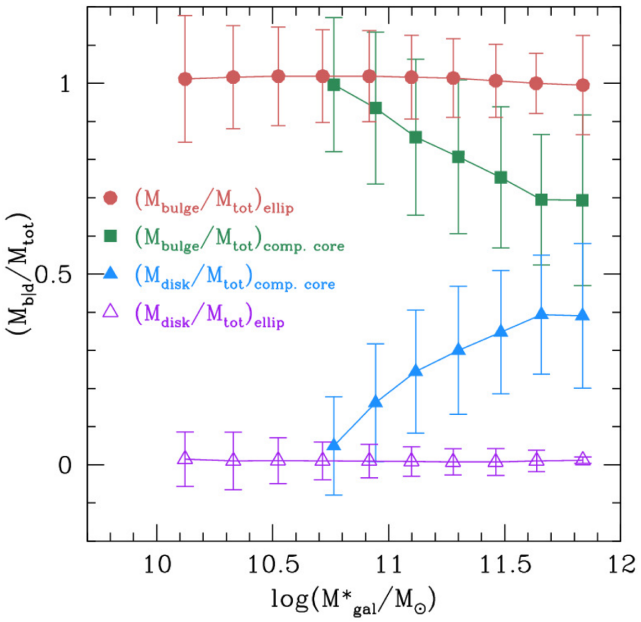

Figure B3. Both compact core and reference elliptical samples, analysed in terms of the mass fraction of their decomposed core (B) and disc (D) structures. A Sérsic $n = 4$ fitting law is used. Elliptical galaxies (red circles and open purple triangles) show the expected behaviour of B/T ~ 1 galaxies. The galaxies hosting compact cores show that the disc/halo accounts for any mass excess above a typical core mass of $\log(M_{\star,\,\rm core}/M_\odot) \sim 11$.

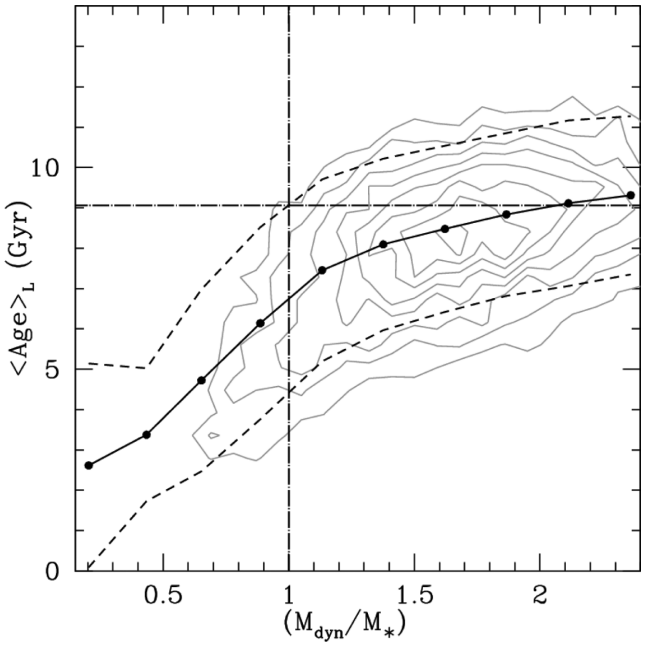

Figure C1. This plot is used to determine a cutoff in $\langle\rm Age\rangle_L$, by demanding $(M_{\rm dyn}/M_\star) \geq 1$. Density contours replace the individual points, while connected filled dots represent the median values in $(M_{\rm dyn}/M_\star)$ bins, with dashed lines outlining the 1σ rms dispersion around the median. At $(M_{\rm dyn}/M_\star) = 1.0$, a rather conservative $\langle\rm Age\rangle_L + 1\sigma = 9.05$ Gyr cutoff value has been obtained.

elliptical galaxies are predominantly extended, only 4.5 per cent of them being compact. For the extended cores, the discrepancy between core sizes measured with free-n and $n = 4$ amounts to 0.05 ± 0.02 dex, less than half the offset measured for compact cores (see Fig. B1)

Finally, Fig. B3 shows the variation with total mass of the mass fraction contained in the discs and bulges of our two SDSS samples: compact cores and reference ellipticals. As expected from the selection rules, the ellipticals have (B/T) ~ 1 and nearly all their mass is packed in the extended cores. Galaxies hosting a compact core show a distinct behaviour in which the more massive the galaxy is, the more relevant the disc/halo becomes. In the frame of our hypothesis, this behaviour is compatible with galaxies having a central, prototypical compact core of $M_{\star,\,\rm core} \sim 10^{11}\,M_\odot$, embedded in an accreted disc/halo (whose mass accounts for any excess above the core mass).

APPENDIX C: CORE CONTAMINATION BY DISC LIGHT

In face-on galaxies, contaminant disc light entering the fibre aperture does not contribute to the velocity dispersion broadening of the core (i.e. dynamical mass), but contributes to the core stellar mass. Therefore, disc contaminated cores tend to show an *unphysical* $M_{\star,\,\rm core} > M_{\rm dyn,\,core}$. In principle, to minimize disc contamination, we could restrict σ measurements to cores in which the SDSS fibre radius (1.5 arcsec) was smaller than the core effective radius. This would, however, be a deficient strategy because the core light profile frequently gets submersed below the disc before attaining its half-light radius. For instance, cores with $R_{\rm e} \lesssim 1.5$ arcsec could still be contaminated. Our approach to avoid light contamination is based on the simple fact that disc light originates in much younger stellar populations than those from the core (e.g. Sánchez-Blázquez 2016, and references therein). Light from a recent star formation event on top of an essentially old core star formation history is an indication of disc light contamination. Instead of using colours, we adopt the luminosity-weighted age $\langle\rm Age\rangle_L$ as a more sensitive parameter to detect disc light contamination.

We have carried out a stellar population study in which average ages (e.g. $\langle\rm Age\rangle_L$) and metallicities are obtained through spectral fitting, using the STARLIGHT synthesis code (Cid Fernandes et al. 2005) to find the optimal mixture of simple stellar populations (SSPs) that describes an SDSS spectrum. For the present study, the basis SSPs correspond to 114 solar-scaled MILES models (Vazdekis et al. 2010). These models have a Kroupa universal IMF (Kroupa 2001) and span a range of six metallicities, from $Z/Z_\odot = 1/50$ to 1.6, and 19 different ages, from 0.5 to 12.6 Gyr. The fitting interval spans from 4000 to 5500 Å, with emission lines and bad pixels being masked out. The extinction due to foreground dust is modelled with the CCM law (Cardelli, Clayton & Mathis 1989). Since the SDSS pipeline does not compute velocity dispersions for spectra with significant emission lines (as for some disc galaxies), we have also used the STARLIGHT spectral fitting to compute our own velocity dispersion values.

Fig. C1 shows the relation between the $\langle\rm Age\rangle_L$ and the $M_{\rm dyn}/M_\star$ ratio for a mixed sample of our compact cores and reference ellipticals (29 482). Individual points have been replaced by density contours and the connected filled dots represent the median values in bins of $M_{\rm dyn}/M_\star$, with dashed black lines outlining the 1σ rms dispersion around the median. The relation supports the idea that unphysical $M_{\rm dyn}/M_\star < 1$ values are connected to low $\langle\rm Age\rangle_L$ values, i.e. disc contamination. A rather conservative cut has been worked out to prevent core contamination, by selecting the $\langle\rm Age\rangle_L + 1\sigma = 9.05$ Gyr at which the $M_{\rm dyn}/M_\star$ ratio becomes larger than unity.

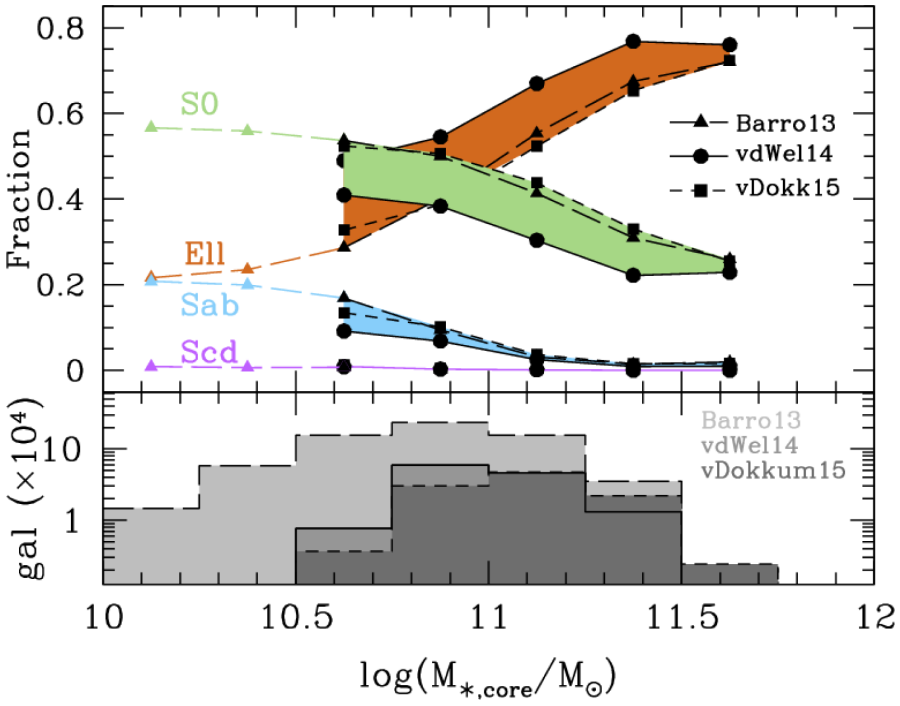

Figure D1. A similar plot to Fig. 8, but using compact core mass $M_{\star,\,\mathrm{core}}$ as the x-axis. Morphology refers to the host galaxies while mass corresponds to the compact cores.

APPENDIX D: ALTERNATIVE MORPHOLOGY RESULTS

Fig. 8 displays one of the most important results of the present study. However, an alternative perspective to that result is presented here. using $M_{\star,\,\mathrm{core}}$ instead of the $M_{\star,\,\mathrm{host}}$. In this case, Fig. D1, the plot shape does not change substantially, but it is roughly shifted with respect to those using $M_{\star,\,\mathrm{host}}$. The mean $\log(M_{\star,\,\mathrm{host}}) - \log(M_{\star,\,\mathrm{core}})$ is 0.25 dex, so morphology fractions of host galaxies with cores in the $\log(M_{\star,\,\mathrm{core}}) = 10.75$–11 bin should be compared with those in the $\log(M_{\star,\,\mathrm{host}}) = 11$–11.25 bin. It is worth emphasizing that the integrated results of Fig. D1 are identical to those in Table 4, because the integration mixes all the galaxies with either $\log(M_{\star,\,\mathrm{host}})$ or $\log(M_{\star,\,\mathrm{core}}) \geq 10.5$.

This paper has been typeset from a TEX/LATEX file prepared by the author.